Geomechanics and Engineering, *Vol. 25, No. 4 (2021) 295-302*
DOI: https://doi.org/10.12989/gae.2021.25.4.295

Investigation on moisture migration of unsaturated clay using cross-borehole electrical resistivity tomography technique

Jiang Lei[1,2a], Weizhong Chen[*1], Fanfan Li[1], Hongdan Yu[1], Yongshang Ma[1] and Yun Tian[**1]

[1]*State Key Laboratory of Geomechanics and Geotechnical Engineering, Institute of Rock and Soil Mechanics, Chinese Academy of Sciences, Wuhan, Hubei 430071, China*
[2]*Shaanxi Provincial Expressway Construction Group Co., Xian, Shaanxi 710065, China*

(Received September 25, 2020, Revised April 26, 2021, Accepted May 8, 2021)

Abstract. Cross-borehole electrical resistivity tomography (ERT) is an effective groundwater detection tool in geophysical investigations. In this paper, an artificial water injection test was conducted on a small clay sample, where the high-resolution cross-borehole ERT was used to investigate the moisture migration law over time. The moisture migration path can be two-dimensionally imaged based on the relationship between resistivity and saturation. The hydraulic conductivity was estimated, and the magnitude ranged from 10^{-11} m/s to 10^{-9} m/s according to the comparison between the simulation flow and the saturation distribution inferred from ERT. The results indicate that cross-borehole ERT could help determine the resistivity distribution of small size clay samples. Finally, the cross-borehole ERT technique has been applied to investigate the self-sealing characteristics of clay.

Keywords: cross-borehole electrical resistivity tomography; unsaturated clay; moisture migration, fracture self-sealing

1. Introduction

Deep underground excavation for the radioactive waste repositories in argillaceous clay may cause damage to the tunnel structures, resulting in fractures that tend to propagate due to the stress redistribution and affect the permeability of the clay. However, the favorable self-sealing characteristics of the clay can help self-sealing its fractures and gradually restore its initial permeability through the swelling of clay minerals, i.e., smectite, interacting with water (Zhang 2013, Labiouse *et al*. 2009, Van Geet *et al*. 2008). Under a specific stress condition, the extent of fracture closure is determined by the clay-water interaction. Thus, the self-sealing of fractured clay can be represented by the re-saturation processes and consequently evaluated by the saturation distribution and moisture migration.

An effective non-invasive electrical resistivity tomography (ERT) technique has been used to investigate the moisture migration law and the saturation process in unsaturated clay (Daily *et al*. 1992). As the direct indicator of its conductivity, clay resistivity is determined by the water content, saturation, ion concentration, and density (Rhoades *et al*. 1976). With other factors remaining constant, the relationship between water content and resistivity can be determined, and the moisture migration can be obtained. The validity of ERT in monitoring water movement is based on the empirical, semi-empirical (Archie 1942), or established in-situ relationships (Farzamian *et al*. 2015a, b) between water content and resistivity. Several studies were conducted to monitor the salt tracer tests or the water infiltration through the unsaturated zones (Rosqvist *et al*. 2000, Audebert *et al*. 2016, Chambers *et al*. 2004, Liu *et al*. 2008, Lee *et al*. 2019, Jo *et al*. 2019). Hassan *et al*. (2013) confirmed that the ERT could be adopted to detect the fractures and investigate the evolution of fractures in clays.

The mounting positions of ERT electrodes vary from on the ground surface, cross-borehole to both on the ground surface and cross-borehole. The high density cross-borehole ERT has been proven most effective. Daily *et al*. (1992) discussed the validity of the cross-borehole ERT when adopting it to study the water flow features in the deep vadose zone. Since then, many scholars began to apply the cross-borehole ERT to monitor the dilution and displacement of a saline tracer plume equipped with electrodes in the borehole (Slater *et al*. 2000, Binley *et al*. 2002, French *et al*. 2002, Wilkinson *et al*. 2010, Bellmunt *et al*. 2016, Perri *et al*. 2012). Similar tests on solute transport properties focused on gaseous CO_2 release in a shallow sand aquifer, meanwhile the elevated water electrical conductivity and CO_2 migration were captured with the cross-borehole ERT (Yang *et al*. 2015 and Dafflon *et al*. 2012). Li *et al*. (2014) adopted the cross-borehole ERT to predict the geological and geotechnical conditions and detected the undesirable clay bodies before tunneling.

In this paper, an artificial water injection test based on the cross-borehole ERT was conducted on a small-size clay sample. The resistivity distribution is derived from the

∗Corresponding author, Professor
E-mail: wzchen@whrsm.ac.cn
∗∗Corresponding author, Ph.D.
E-mail: tianyun_2016@163.com
[a]Ph.D.
E-mail: leiucas2014@163.com

ISSN: 2005-307X (Print), 2092-6219 (Online)

corresponding data inversion. During clay saturation, the saturated zone expands, and the pore space is gradually filled by water due to the moisture migration, resulting in resistivity distribution changes. Thus, resistivity measurement is effective in evaluating the distribution of moisture content in clays. In the meantime, the hydraulic conductivity can be estimated by comparing the results of unsaturated flow simulation and the saturation derived from the ERT.

2. Experimental details

2.1 Material and sample preparation

The tests was conducted on a remolded clay sample. In natural clays, the volume porosity is 39 % on averagely and water content ranges from 24 % to 30 %. The clay minerals include illites, smectites and kaolinites, accounting for about 60 % of the total mass. The non- clay minerals include quartz (about 25 %), feldspar, and a little pyrite and calcite (Yu *et al*. 2012). The sample was remolded with clay powders and synthetic clay water (SCW) under a total stress state of 4.5 MPa. Table 1 lists the main characteristics of the tested sample. A 5 mm × 40 mm groove was made on the sample, as shown in Fig. 1.

The synthetic clay water (SCW) is configured according to the aqueous composition of the clay rock in situ. The main components are NaCl and $CaCO_3$. The solution was stirred for 72h before injected into a back pressure generator and was deaired with a vacuum pump for 1h (Gong 2015).

2.2 Experimental apparatus

The experimental apparatus consists of the multi-core cable, the power supply module, microelectrodes, the data acquisition module, and the intelligent conversion module, as shown in Fig. 2. The apparatus also adopts the FlashRES64 system, characterized by multi-channel, ultra-high density and direct current prospecting inversion. Data was collected through the electrode conversion, and the results of resistivity distribution were determined through the inversion, which are much close to the real state. The apparatus has many advantages, including good stability, high efficiency, and high resolution, all of which helped improve the reliability of the results.

2.3 Experimental procedure

The experimental apparatus comes with 64 channels, and 24 of which were adopted in the test due to the size of the clay sample. The electrodes symmetrically installed on the two sides of clay sample along the axial direction with the interspacing of 6 mm were labeled 1 to 12 and 53 to 64. All electrodes were connected to the intelligent conversion module through the multi-core cable, as shown in Fig. 3. Throughout the test, the groove was maintained full of synthetic clay water.

The test was conducted in the following steps:

Step 1: Assembling the apparatus modules and installing the electrodes;

Step 2: Setting the voltage, electrode space, and other configurations;

Step 3: Grouping the electrodes. Two power supply electrodes are driven by a known current and the voltage

Table 1 Parameters of the tested sample

Parameter	D_0 (mm)	H_0 (mm)	W_0 (%)	ρ_{d0} (g/cm^3)	ρ_0 (g/cm^3)	Sr
Value	80	100	16.96	1.7	2.01	0.7

*D_0 is the diameter, H_0 is height, ρ_0 is density, ρ_{d0} is the dry density, W_0 is water content, Sr is saturation degree

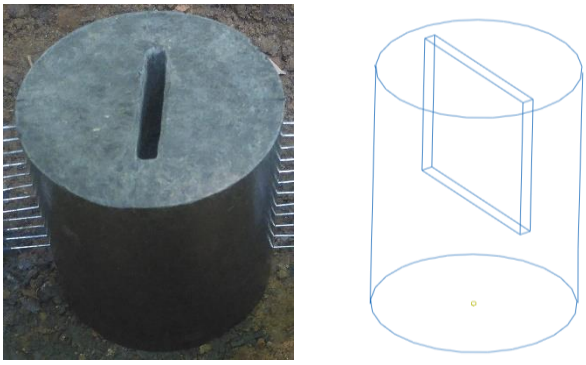

(a) Physical map (b) Sketch map

Fig. 1 The cylindric clay sample with a groove

Fig. 2 The FlashRES64 system

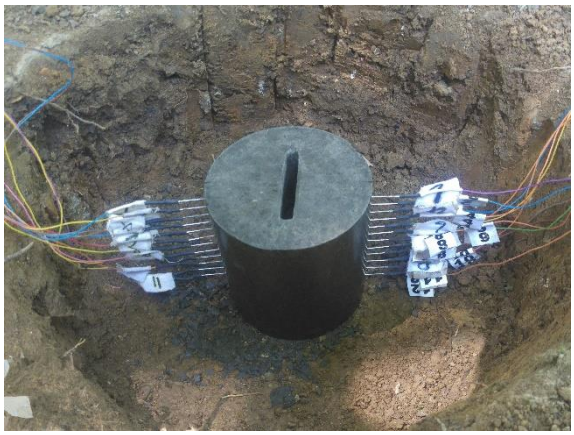

Fig. 3 The Layout electrodes

difference is measured between all other pairs of electrodes. Then, the known current is applied to two other electrodes and the voltage is again measured between all other pairs. This process is repeated until current has been applied to all pairs of electrodes;

Step 4: Measuring and recording the voltages on the electrode;

Step 5: Ensuring steps 2 to 4 are completed within a fixed time.

2.4 Electrical resistivity method

When point power source A is on the earth surface, the underground space is treated as semi- infinite space. Assuming that the underground medium is homogeneous, the potential of the direct current field satisfies the following basic differential equation (Li 2008):

$$\nabla\bullet(\sigma\nabla U)=-2I\delta(A) \qquad \in\Omega \tag{1}$$

where σ is the electrical conductivity, I is the power supply current, and δ(A) is the Kronecker function centered at point A.

The potential of the direct current field also satisfies the following boundary conditions:

$$\begin{aligned} &\frac{\partial U}{\partial n}=0 && \in\Gamma_S \\ &\frac{\partial U}{\partial n}+\frac{\cos(r,n)}{r}U=0 && \in\Gamma_\infty \end{aligned} \tag{2}$$

where U is the potential of electric field, n is the normal direction of earth surface, r is the distance to point A, Γ_s is the surface boundary, Γ_∞ is the infinite boundary.

Thousands of data were derived from a cycle of measurement, during which the unfavorable data were eliminated by the certain standards. The ERT data were inverted in RES2DINV software with the least square method. The inverted results were much close to the actual resistivity of the clay sample thanks to the large amount of data and the high resolution instrument. As an important factor influencing the measurement of resistivity, the temperature was monitored with a thermometer to help obtain more accurate data during the tests.

2.5 The relationship between saturation and resistivity

The resistivity of the clay sample was measured under different saturations of 0.9, 0.7, 0.5 and 0.3 to investigate the resistivity variation law with saturation. The samples with the same dry density were remolded with clay powders and SCW under the stress state of 4.5 MPa.

The resistivity was measured using the same method as the artificial water injection test. The relationship between saturation and resistivity was shown in Fig. 4. The relationship between the resistivity and saturation can be expressed as Eq. (3), which is based on Archie (1942), Farzamian *et al*. (2015a). The error of Eq. (3) is 0.69%. This error is evaluated by the mean absolute percent error (MAPE) (Beyer 1991). This MAPE is a well-known index

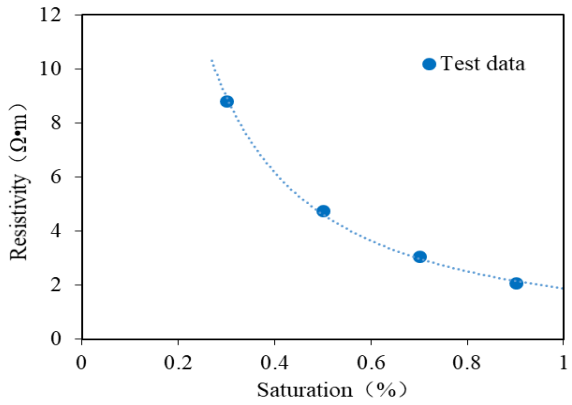

Fig. 4 Relationship between saturation degree and resistivity

to quantify the error between the experimental results and predicted results.

$$\rho=1.8749*\mathrm{Sr}^{-1.312} \tag{3}$$

where ρ is the resistivity; Sr is the degree of saturation.

As shown in Fig. 4, the resistivity of the samples tends to decrease with the increase of saturation degree. The reason behind this trend is that the pore space within the samples was filled with more water due to the increasing saturation degree, which led to an increased amount mobile ions and consequently the increased conductivity. However, when the saturation degree is over a specific value, the connectivity of the pores within the samples becomes better. With the increase of the moisture content, the number of mobile ions and connectivity show no significant change. Thus, the resistivity tends to decrease by a lower amplitude.

2.6 Moisture migration simulation

The moisture migration was simulated in the ABAQUS software. Two-dimensional Richards' equation can be expressed as,

$$\frac{\partial}{\partial x}(k_x\frac{\partial h}{\partial x})+\frac{\partial}{\partial x}(k_y\frac{\partial h}{\partial y})=\frac{\partial\theta_w}{\partial t} \tag{4}$$

where k_x and k_y are the hydraulic conductivity of x and y directions, respectively; θ_w is the water content; h is the total head; t is time.

Substituting $\partial\theta_w=m_w\partial u_w=m_w\gamma_w\partial(h-y)$ into the Eq. (4), and let y be the position head, then $h=\frac{u_w}{\gamma_w}+y$.

$$\frac{\partial}{\partial x}(k_x\frac{\partial h}{\partial x})+\frac{\partial}{\partial x}(k_y\frac{\partial h}{\partial y})=\frac{m_w\gamma_w\partial(h-y)}{\partial t} \tag{5}$$

3. Results and discussions

3.1 The resistivity evolution

The saturation process was measured during the first 15

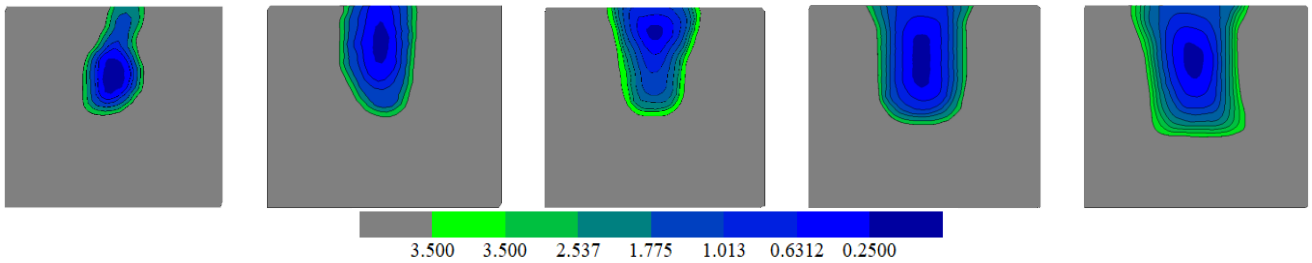

(a) t=3600s (b) t=7200s (c)t=12600s (d) t=28800s (e) t=54000s

Fig. 5 Resistivity distribution at different time

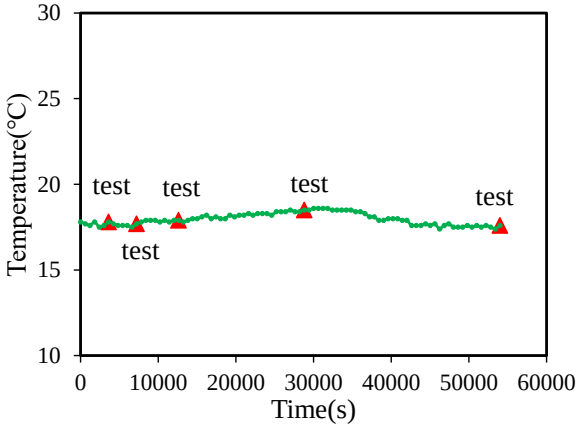

Fig. 6 Relationship between temperature and time

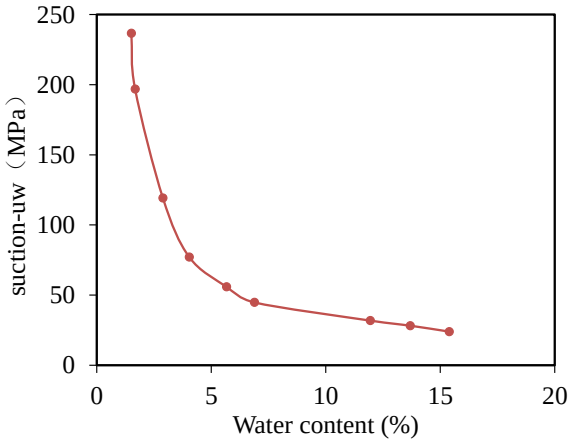

Fig. 8 The soil-water characteristic curve

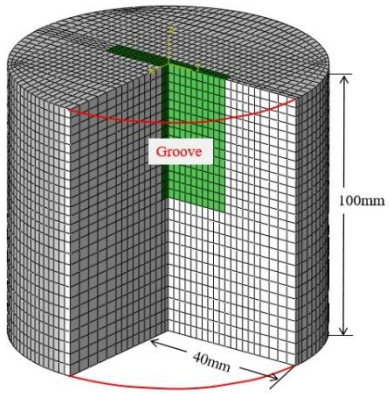

Fig. 7 The 3D FEM mesh of the model

hours. The inversion of ERT data was conducted in the RES2DINV software (Loke 2004). The RMS (Root-Mean-Square) error varied from 5% to 15%. These results suggest a rather good fit with the model, especially when considering the possible strong 2D resistivity effect.

Five measurements were made during the artificial water injection test, the distribution of resistivity was obtained, and the low resistance areas were identified. Fig.5 shows the results of resistivity imaging at different times, where the blue and grey areas represent the low and initial high resistivity zones, respectively. The images show that the low resistivity area appears in the center of the sample because the groove is filled with saline water. Thus, it is concluded that:

(1) The water in the groove can be detected within the small-size sample with the cross-borehole ERT, and some good results can be obtained.

(2) The resistivity of the sample approximates 3.5 $\Omega \cdot m$ when the initial saturation is 0.7, and the zone where the resistivity is below 3.5 $\Omega \cdot m$ is the seepage area in which the saturation is over 0.7.

(3) The low resistivity zone in the centre of sample represents the location of groove or fracture, which is filled with saline water.

(4) The low resistivity zone expands gradually, indicating that water migrates from the groove to the surrounding areas, and the vadose zone constantly absorbs water.

The temperatures varied within 1 degree, as shown in Fig. 6, indicating that temperature has little effect on the measurement of resistivity, thus can be ignored during the test.

3.2 Estimating the hydraulic conductivity of clay

Hydraulic conductivity is critical for determining the potential of water migration. The water injection test was simulated in the ABAQUS software, and the results of unsaturated flow simulation and the saturation results acquired through ERT were compared. The saturation process was simulated under different hydraulic conductivity levels, i.e., 10^{-8} m/s, 10^{-9} m/s, 10^{-10} m/s, and 10^{-11}m/s.

The model is shown in Fig. 7. The diameter and height of the model are 80 mm and 100mm, respectively. There are 31428 elements (C3D8RP) and 34244 nodes. The normal deformation is fixed in the boundaries except the top surface of the model. The stress is initialized according to

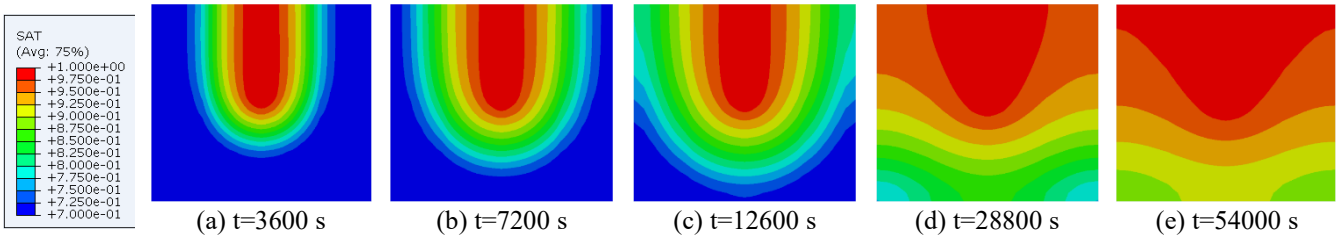

(a) t=3600 s (b) t=7200 s (c) t=12600 s (d) t=28800 s (e) t=54000 s

Fig. 9 Saturation degree distribution over time at the hydraulic conductivity of 10^{-8} m/s

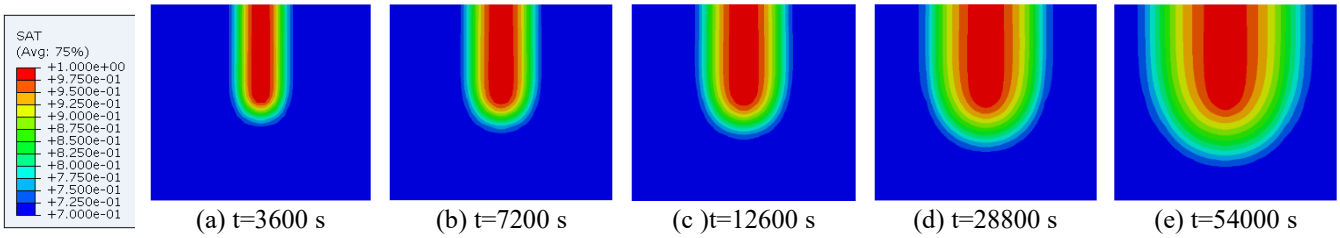

(a) t=3600 s (b) t=7200 s (c)t=12600 s (d) t=28800 s (e) t=54000 s

Fig. 10 Saturation degree distribution over time at the hydraulic conductivity of 10^{-9} m/s

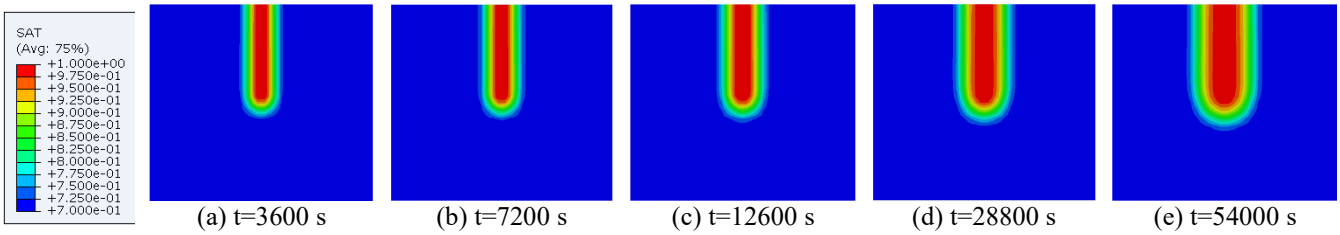

(a) t=3600 s (b) t=7200 s (c) t=12600 s (d) t=28800 s (e) t=54000 s

Fig. 11 Saturation degree distribution over time at the hydraulic conductivity of 10^{-10}m/s

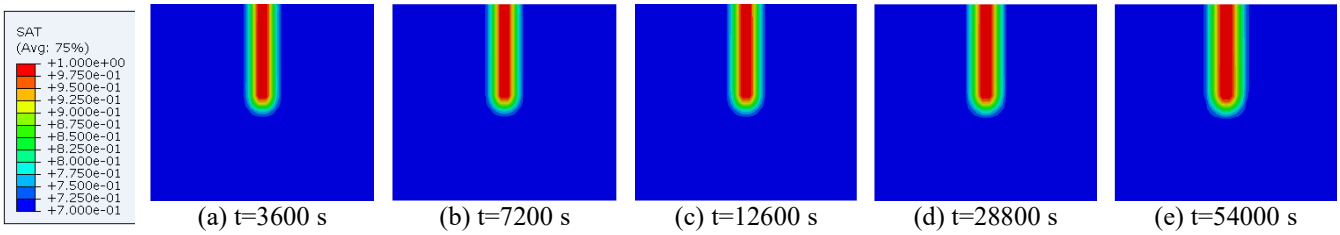

(a) t=3600 s (b) t=7200 s (c) t=12600 s (d) t=28800 s (e) t=54000 s

Fig. 12 Saturation degree distribution over time at the hydraulic conductivity of 10^{-11}m/s

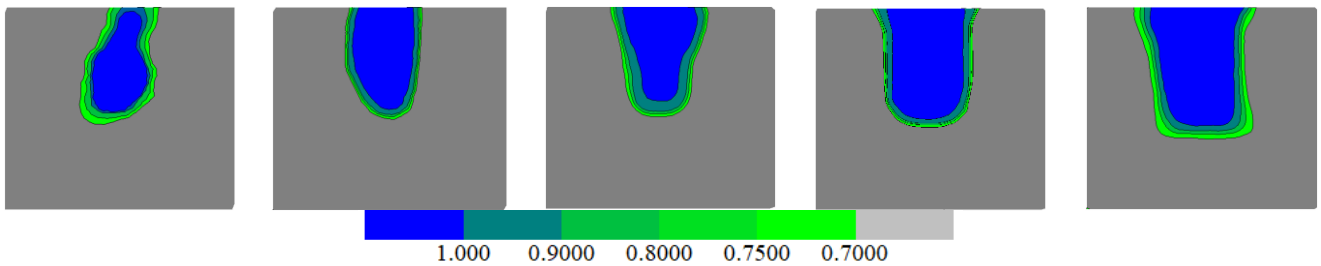

(a) t=3600s (b) t=7200 s (c) t=12600 s (d) t=28800 s (e) t=54000 s

Fig. 13 Saturation distribution converted from RET data

height direction and the pore water pressure is initialized according to soil-water characteristic curve (Bernier *et al*. 1997). The modelling procedure was divided into the following two phases: the first is in-situ tress equilibrium phase, the second is seepage phase (15 hours), including removing the element of groove and activating pore water pressure and boundary condition of groove.

Fig. 8 shows the soil-water characteristic curve of the remolded sample (Bernier *et al*. 1997). The relationship between water permeability and saturation degree is depicted with reference to Romero (1999). Water migrates from the fractures to the vadose zone. Thus, the distribution of saturation at different times can be obtained, and the hydraulic conductivity can be estimated.

Figs. 9-13 show the distribution of the simulated saturation degree in the ABAQUS software under different

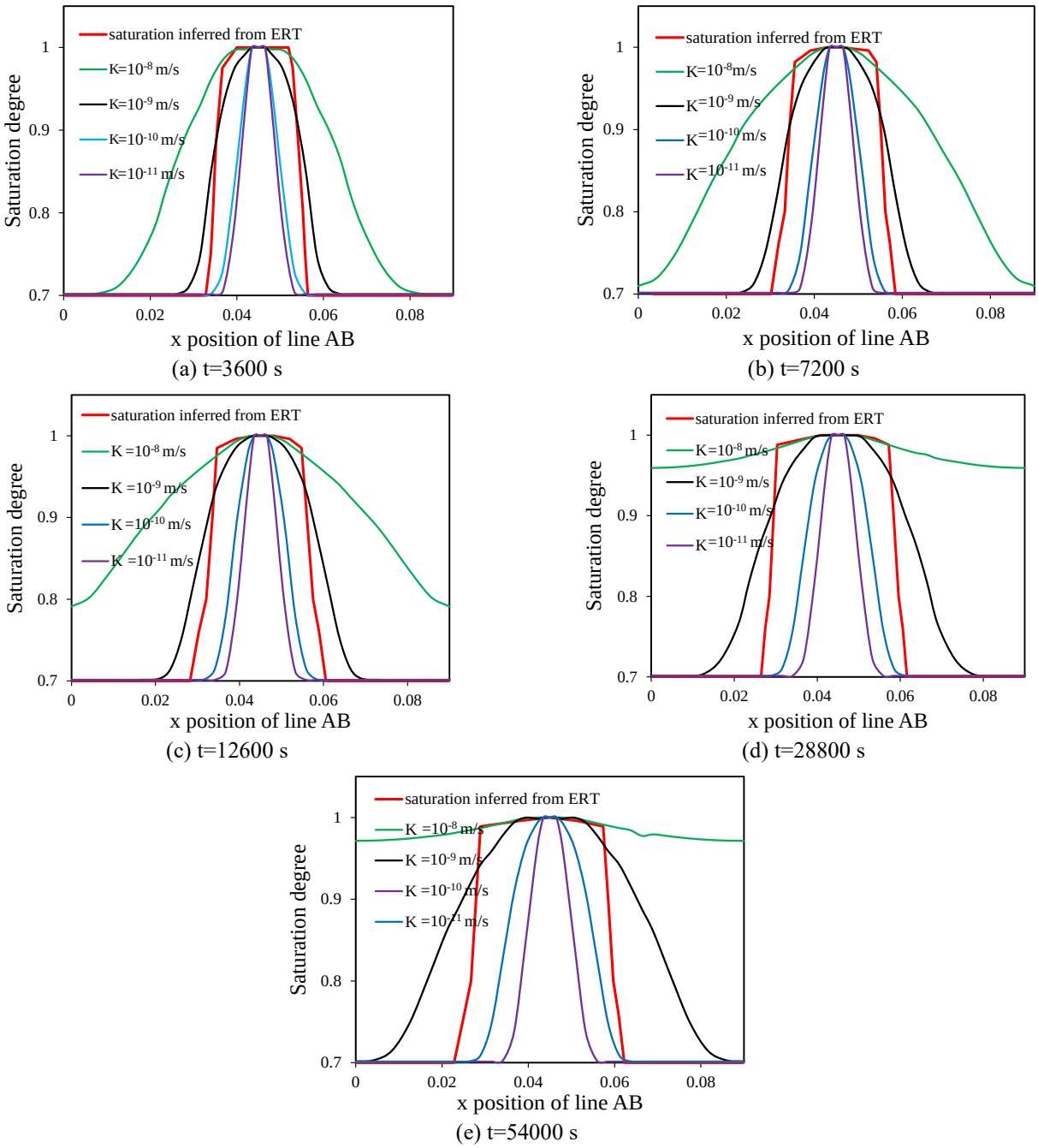

Fig. 14 Saturation distribution on line AB at different time

hydraulic conductivity and the saturation degree acquired through RET. The distributions of saturation are similar to the simulation results under the hydraulic conductivity of 10^{-9} m/s.

A horizontal line AB in the middle of the groove was drawn to study the relationship between the sets of results. The saturation degree distribution on line AB was plotted in Fig. 14, which shows that the higher the hydraulic conductivity, the greater the saturation. The saturation distribution acquired through ERT lies within the range of 10^{-9} to10^{-10} m/s. The hydraulic conductivity of the original clay approximates 10^{-12} m/s (Van Geet *et al*. 2008) due to the intact structure and the over-consolidated soil. Thus, the hydraulic conductivity of the remolded sample is 2 orders of magnitude lower than the undisturbed sample.

The hydraulic conductivity of the saturated remolded clay sample was measured by the steady state method, and the test curve is shown in Fig.15. The measured hydraulic conductivity is $2.82*10^{-10}$m/s, which conforms to the estimation range of 10^{-9} to10^{-10} m/s.

3.3 Discussion

Farzamian *et al*. (2015b) compared the simulated flow with the moisture distribution acquired through ERT, and one misfit error value was used to evaluate which hydraulic conductivity value best represents the field conditions. In this paper, the simulated results were compared with the test

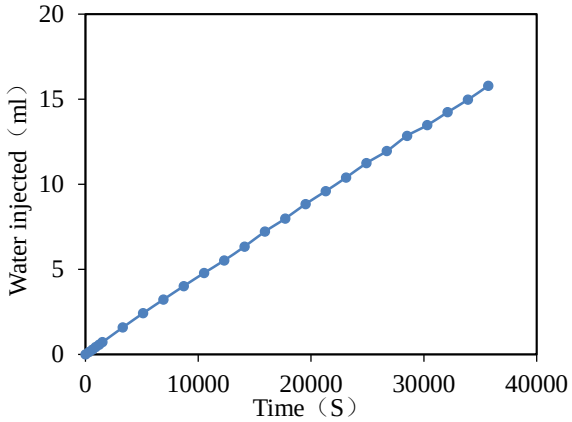

Fig. 15 Injected water flow-time relationship of the steady-state experiment on the saturated remolded clay

Fig. 16 Schematic of the clay sample after testing

results of one key cross section, and one penetration test was conducted to confirm its reasonability. The two-dimensional distribution of apparent resistance can be acquired through cross-borehole ERT. The evolution law of apparent resistance represents the water migration. The RMS (Root-Mean-Square) error is reasonable, ranging from 5% to 15%. With good consistency to the test data, ERT can be applied to analyze the evolution law of water migration in mudstone. However, two-dimensional inversion techniques were adopted for data processing due to the immaturity of three-dimensional inversion techniques and the limited sample size. Therefore, the test results can provide some good examples for the investigation of water migration in mudstone. Due to the inadequacy of data processing, the theory of three-dimensional resistance inversion technique also needs developing in the future.

Fig. 16 shows the schematic of the clay sample after testing. The initial empty groove was filled with clay particles under the action of hydration swelling after more than ten hours. The permeability of the fracture decreased because of the reduction of seepage channel, which indicates that the fracture has a certain degree of closure. Although it is difficult to use hydraulic conductivity or other index to quantitatively characterize the degree of closure in this paper, it is observed that fracture self-sealing process occur due to the hydration swelling.

The self-sealing characteristics are important to evaluate the safety of the nuclear waste disposal repository. Also, water is one of the most important factors influencing the self-sealing characteristics (Zhang 2013, Labiouse *et al*. 2009, Van Geet *et al*. 2008). The excavation of the disposal repository would cause fractures and improve the permeability of clays. The surrounding rock gradually becomes saturated after support. And the clay absorbs the water and generates the swelling strain to minimize the degree of fracture. Water content and self-sealing capacity have a specific relationship, and the higher the saturation, the easier the fracture closure. Therefore, through this study, we intend to apply ERT technique to the field to study the moisture migration in the process of re-saturation of surrounding rock after excavation of gallery of disposal system. The results of water distribution acquired through ERT can be used to guide and evaluate the studies of the fracture self-sealing. However, the evaluation of self-sealing degree is a qualitative description because there are almost no similar studies using specific function expressions to describe the relationship between water and self-sealing capacity quantitatively. Additionally, relevant tests are required to investigate the relationship between water and self-sealing, and a self-sealing model considering water should be built to evaluate and simulate the self-sealing of fractured clays.

4. Conclusions

The artificial water injection test was conducted on the clay sample, and the moisture migration law was investigated through cross-borehole ERT during the saturation. The following conclusions are obtained:

- The low resistivity zone can be detected and the distribution of resistivity can be obtained through the cross-borehole ERT, which confirms its suitability for the small-size samples.
- The saturation process can be obtained based on the distribution of resistivity and the saturation acquired through ERT.
- An important parameter of hydraulic conductivity is estimated based on the comparison between simulated water flow and the saturation distribution acquired through ERT.
- Water is critical for the self-sealing characteristic. The distribution of saturation can be quantified through experimental studies. The cross-borehole ERT technique can be employed in the field to determine the water migration and evaluate the self-sealing capacity of fractured clays.

Acknowledgments

The authors gratefully acknowledge the financial support from the National Natural Science Foundation of China [No. 51979266] and the National Natural Science Foundation of China [No. 51879258] to this research.

References

Archie, G.E. (1942), “The electrical resistivity log as an aid in determining some reservoir characteristics”, *Trans. AIME*,

146(1), 54-62. https://doi.org/10.2118/942054-G.

Audebert, M., Oxarango, L., Duquennoi, C., Touze-Foltz, N., Forquet, N. and Clément, R. (2016), "Understanding leachate flow in municipal solid waste landfills by combining time-lapse ERT and subsurface flow modelling–Part II: Constraint methodology of hydrodynamic models", *Waste Manage*., **55**, 176-190. https://doi.org/10.1016/j.wasman.2016.04.005.

Bellmunt, F., Marcuello, A., Ledo, J. and Queralt, P. (2016), "Capability of cross-hole electrical configurations for monitoring rapid plume migration experiments", *J. Appl. Geophys*., **124**, 73-82. https://doi.org/10.1016/j.jappgeo.2015.11.010.

Bernier, F., Volckaert, G., Alonso, E. and Villar, M. (1997), "Suction-controlled experiments on Boom clay", *Eng. Geol*., **47**(4), 325-338. https://doi.org/10.1016/S0013-7952(96)00127-5.

Beyer, W. H. (1991), *CRC Standard Mathematical Tables and Formulae*, CRC Press, Boca Raton, Florida, U.S.A.

Binley, A., Cassiani, G., Middleton, R. and Winship, P. (2002), "Vadose zone flow model parameterisation using cross-borehole radar and resistivity imaging", *J. Hydrol*., **267**(3-4), 147-159. https://doi.org/10.1016/S0022-1694(02)00146-4.

Chambers, J.E., Loke, M.H., Ogilvy, R.D. and Meldrum, P.I. (2004), "Noninvasive monitoring of DNAPL migration through a saturated porous medium using electrical impedance tomography", *J. Contam. Hydrol*., **68**(1-2), 1-22. https://doi.org/10.1016/s0169-7722(03)00142-6.

Dafflon, B., Wu, Y., Hubbard, S.S., Birkholzer, J.T., Daley, T.M., Pugh, J.D. and Trautz, R.C. (2013), "Monitoring CO2 intrusion and associated geochemical transformations in a shallow groundwater system using complex electrical methods", *Environ. Sci. Technol*., **47**(1), 314-321. https://doi.org/10.1007/s12665-012-2168-z.

Daily, W., Ramirez, A., LaBrecque, D. and Nitao, J. (1992), "Electrical resistivity tomography of vadose water movement", *Water Resour. Res*., **28**(5), 1429-1442. https://doi.org/10.1029/91WR03087.

Farzamian, M., Santos, F.A.M. and Khalil, M.A. (2015a), "Estimation of unsaturated hydraulic parameters in sandstone using electrical resistivity tomography under a water injection test", *J. Appl. Geophys*., **121**, 71-83. https://doi.org/10.1016/j.jappgeo.2015.07.014.

Farzamian, M., Santos, F.A.M. and Khalil, M.A. (2015b), "Application of EM38 and ERT methods in estimation of saturated hydraulic conductivity in unsaturated soil", *J. Appl. Geophys*., **112**, 175-189. https://doi.org/10.1016/j.jappgeo.2014.11.016.

French, H.K., Hardbattle, C., Binley, A., Winship, P. and Jakobsen, L. (2002), "Monitoring snowmelt induced unsaturated flow and transport using electrical resistivity tomography", *J. Hydrol*., **267**(3-4), 273-284. https://doi.org/10.1016/S0022-1694(02)00156-7.

Gong, Z. (2015), "Long-term thermo-hydro-mechanical coupled behaviour of Belgium Boom clay". Ph.D. Dissertation, The University of Chinese Academy of Sciences, Beijing, China.

Hassan, A. and Toll, D.G. (2013), "Electrical resistivity tomography for characterizing cracking of soils", *Geotech. Sp. Publ*., **231**, 818-827. https://doi.org/10.1061/9780784412787.083.

Jo S.A., Kim K.Y. and Ryu H.H. (2019), "A new geophysical exploration method based on electrical resistivity to detect underground utility lines and geological anomalies: Theory and field demonstrations", *Geomech. Eng*., **18**(5), 527-534. http://doi.org/10.12989/gae.2019.18.5.527.

Labiouse, V., Escoffier, S., Gastaldo, L. and Mathier, J.F. (2009), "Self-sealing of localised cracks in boom and opalinus clay hollow cylinders", *Proceedings of the European Commission TIMODAZ-THERESA Conference*, Luxembourg, Germany, September.

Lee, K. H., Park, J.H., Park, J., Lee, I.M. and Lee, S.W. (2019), "Electrical resistivity tomography survey for prediction of anomaly in mechanized tunneling" *Geomech. Eng*., **19**(1), 93-104. http://doi.org/10.12989/gae.2019.19.1.093.

Li, S., Su, M. and Xue, Y. (2014), "Study on computed tomography of cross-hole resistivity in urban subway geological prediction", *Chin. J. Rock Mech. Eng*., **33**(5), 913-920.

Li, T.C. (2008), "2D, 3D forward modeling and inversion research of resistivity tomography technique". Ph.D. Dissertation, China University of Geosciences, Beijing, China.

Liu, H.L., Zhou, Q.Y. and Wu, H.Q. (2008), "Laboratorial monitoring of the LNAPL contamination process using electrical resistivity tomography", *Chin. J. Geophys*., **51**(4), 883-891. https://doi.org/10.1002/cjg2.1282.

Loke, M.H. (2004), Tutorial: 2-D and 3-D Electrical Imaging Surveys, Geotomo Software, Malaysia. https://www.geoelectrical.com.

Perri, M.T., Cassiani, G., Gervasio, I., Deiana, R. and Binley, A. (2012), "A saline tracer test monitored via both surface and cross-borehole electrical resistivity tomography: Comparison of time-lapse results", *J. Appl. Geophys*., **79**, 6-16. https://doi.org/10.1016/j.jappgeo.2011.12.011.

Rhoades, J.D. and Van Schilfgaarde, J. (1976), "An electrical conductivity probe for determining soil salinity", *Soil Sci. Soc. Amer. J*., **40**(5), 647-651. https://doi.org/10.2136/sssaj1976.03615995004000050016x.

Romero, E., Gens, A. and Lloret, A. (1999), "Water permeability, water retention and microstructure of unsaturated compacted Boom clay", *Eng. Geol*., **54**(1-2), 117-127. https://doi.org/10.1016/S0013-7952(99)00067-8.

Rosqvist, H. and Destouni, G. (2000), "Solute transport through preferential pathways in municipal solid waste", *J. Contam. Hydrol*., **46**(1-2), 39-60. https://doi.org/10.1016/S0169-7722(00)00127-3.

Slater, L., Binley, A.M., Daily, W. and Johnson, R. (2000), "Cross-hole electrical imaging of a controlled saline tracer injection", *J. Appl. Geophys*., **44**(2-3), 85-102. https://doi.org/10.1016/S0926-9851(00)00002-1.

Van Geet, M., Bastiaens, W. and Ortiz, L. (2008), "Self-sealing capacity of argillaceous rocks: review of laboratory results obtained from the SELFRAC project", *Phys. Chem. Earth Parts A/B/C*, **33**(s1), S396-S406. https://doi.org/10.1016/j.pce.2008.10.063.

Wilkinson, P.B., Meldrum, P.I., Kuras, O., Chambers, J.E., Holyoake, S.J. and Ogilvy, R.D. (2010), "High-resolution electrical resistivity tomography monitoring of a tracer test in a confined aquifer", *J. Appl. Geophys*., **70**(4), 268-276. https://doi.org/10.1016/j.jappgeo.2009.08.001.

Yang, X., Lassen, R.N., Jensen, K.H. and Looms, M.C. (2015), "Monitoring CO2 migration in a shallow sand aquifer using 3D crosshole electrical resistivity tomography", *Int. J. Greenhouse Gas Control*, **42**, 534-544. https://doi.org/10.1016/j.ijggc.2015.09.005.

Yu, H.D., Chen, W.Z., Jia, S.P., Cao, J.J. and Li, X.L. (2012), "Experimental study on the hydro-mechanical behavior of Boom clay", *Int. J. Rock Mech. Min. Sci*., **53**, 159-165. https://doi.org/10.1016/j.ijrmms.2012.05.013.

Zhang, C.L. (2013), "Sealing of fractures in claystone", *J. Rock Mech. Geotech. Eng*., **5**(3), 214-220. https://doi.org/10.1016/j.jrmge.2013.04.001.

CC